



# Longitudinal Morphometric Changes in the Corticospinal Tract Shape After Hemorrhagic Stroke

Seth B. Boren<sup>1</sup> · Sean I. Savitz<sup>1</sup> · Nicole Gonzales<sup>1,6</sup> · Khader Hasan<sup>4</sup> · Andrea Becerril-Gaitan<sup>2</sup> · Vahed Maroufy<sup>3</sup> · Yuan Li<sup>3</sup> · James Grotta<sup>5</sup> · Emily A Steven<sup>1</sup> · Ching-Jen Chen<sup>2</sup> · Clark W. Sitton<sup>4</sup> · Jaroslaw Aronowski<sup>1</sup> · Muhammad E. Haque<sup>1</sup>

Received: 17 May 2023 / Revised: 6 June 2023 / Accepted: 7 June 2023 / Published online: 13 June 2023  
© The Author(s), under exclusive licence to Springer Science+Business Media, LLC, part of Springer Nature 2023

## Abstract

Deep intracerebral hemorrhage (ICH) exerts a direct force on corticospinal tracts (CST) causing shape deformation. Using serial MRI, Generalized Procrustes Analysis (GPA), and Principal Components Analysis (PCA), we temporally evaluated the change in CST shape. Thirty-five deep ICH patients with ipsilesional-CST deformation were serially imaged on a 3T-MRI with a median imaging time of day-2 and 84 of onset. Anatomical and diffusion tensor images (DTI) were acquired. Using DTI color-coded maps, 15 landmarks were drawn on each CST and the centroids were computed in 3 dimensions. The contralesional-CST landmarks were used as a reference. The GPA outlined the shape coordinates and we superimposed the ipsilesional-CST shape at the two-time points. A multivariate PCA was applied to identify eigenvectors associated with the highest percentile of change. The first three principal components representing CST deformation along the left-right (PC1), anterior-posterior (PC2), and superior-inferior (PC3) respectively were responsible for 57.9% of shape variance. The PC1 (36.1%,  $p < 0.0001$ ) and PC3 (9.58%,  $p < 0.01$ ) showed a significant deformation between the two-time points. Compared to the contralesional-CST, the ipsilesional PC scores were significantly ( $p < 0.0001$ ) different only at the first-timepoint. A significant positive association between the ipsilesional-CST deformation and hematoma volume was observed. We present a novel method to quantify CST deformation caused by ICH. Deformation most often occurs in left-right axis (PC1) and superior-inferior (PC3) directions. As compared to the reference, the significant temporal difference at the first time point suggests CST restoration over time.

**Keywords** Intracerebral hemorrhage · Stroke · Morphometrics · Corticospinal tracts · Diffusion tensor imaging · Serial magnetic resonance imaging · Generalized procrustes analysis · Principal component analysis

✉ Muhammad E. Haque  
Muhammad.E.Haque@uth.tmc.edu

<sup>1</sup> Institute for Stroke and Cerebrovascular Diseases and Department of Neurology, McGovern Medical School, The University of Texas Health Science Center, 6431 Fannin Street, Houston, TX 77030, USA

<sup>2</sup> Department of Neurosurgery, McGovern Medical School, The University of Texas Health Science Center, Houston, USA

<sup>3</sup> Department of Biostatistics and Data Science, School of Public Health, McGovern Medical School, The University of Texas Health Science Center, Houston, USA

<sup>4</sup> Department of Interventional Diagnostic Radiology, McGovern Medical School, The University of Texas Health Science Center, Houston, USA

<sup>5</sup> Stroke Research and Mobile Stroke Unit, Department of Neurology, Memorial Hermann Hospital, Houston, USA

<sup>6</sup> Department of Neurology, Neurohospitalist and Stroke Section, University of Colorado School of Medicine, Aurora, USA

## Introduction

Intracerebral hemorrhage (ICH) accounts for 10–20% of all strokes and carries the highest disability rates among survivors [1]. After ICH, the primary cause of brain injury results from the mechanical force induced by the growing hematoma causing brain tissue compression and a significant increase in intracranial pressure (ICP) [2–4]. Furthermore, the extravasated blood increases toxic components within the brain parenchyma, such as thrombin, proteases, and hemolysis products, which ultimately lead to increased oxidative stress, neuroinflammation, brain blood barrier (BBB) disruption, and edema [5–9].

Among patients with hematoma involving the corticospinal tract (CST), limb impairment remains the primary cause of disability [10–12]. Post-ICH physical rehabilitation is an integral part of clinical care, but the integrity of CST, the primary communication pathway between the motor function and impaired limb, is rarely evaluated via imaging. Several post-ICH imaging studies have shown CST injury and lack of tract continuity, yet we have a poor understanding of the morphological changes to the CST caused by ICH. There is a significant knowledge gap regarding the neuroanatomical changes to the CST. To develop better treatments to promote neurological recovery, we need a better understanding of neuroanatomical distortions to the CST.

Non-invasive diffusion tensor imaging (DTI) has emerged as a key tool for assessing the microstructural integrity of white matter tracts, also known as tractography. It exploits both the magnitude and orientation of water molecules diffusion as a tracer to probe tissue integrity [13–16]. However, tractography has been criticized for being strongly biased. Therefore, the present study leverages a novel concept of morphometric analysis, known as Generalized Procrustes Analysis (GPA), to evaluate the temporal change in CST shape after ICH. GPA is a statistical analysis method used to compare the shape of an object by superimposing and minimizing the Procrustes distance or shape differences [17–22]. Recently, the morphological difference in shape has been used to assess several neurological disorders such as Chiari malformation, restless leg syndrome, mesial temporal sclerosis, and aging [23–26]. To the best of our knowledge, this is the first study evaluating the temporal change in the CST shape and its association with the hematoma size and recovery among patients with ICH.

## Methods

### Patient Enrollment & Human Protection

This study was approved by the institutional review board of the University of Texas Health Sciences Center at Houston and by the Memorial Hermann Hospital Office of Research. In this retrospective analysis, patients were pooled from the 3 serial imaging studies of patients with ICH. Two studies were prospective observational studies and the third was a double-blinded clinical trial testing pioglitazone.

The inclusion criteria for our cohort were spontaneous supratentorial ICH, age 18–80 years, baseline hematoma volume <100 mL and National Institutes of Health Stroke Scale (NIHSS) <25, CST involvement, availability of the DTI at two-time points. Patients with a brain tumor, traumatic brain injury, cerebral aneurysm, arteriovenous malformation, claustrophobia, or metal implantation were excluded. A total of 54 patients were screened and 35 ICH patients were included. The patient enrollment is summarized in Fig 1.

### Neurological and Radiological Assessments

All participants underwent baseline and serial assessment of neurological deficits via the NIHSS. Computed tomography (CT) or magnetic resonance imaging (MRI) was obtained within 6–24 h of ICH onset as part of the standard of care without quantitative MRI. The serial MRIs were obtained with a median time of 2 (V1 = visit1) and 84 (V2 = visit2) days of onset. The qualitative radiological assessment included the presence of a mass effect, midline shift, and the development of Wallerian Degeneration (WD). The quantitative measurement included changes in hematoma volume and the ipsilesional CST shape.

### MRI Data Acquisition

Serial images were obtained using two different Philips and one GE full-body 3.0 T MRI systems because images were obtained both as in and out-patients. Anatomical images included both the 2D and 3D T1-weighted (2D = TR/TE = 600/13 ms, imaging matrix (MTX) = 256 × 256, slice thickness = 5 mm; 3D = TR/TE = 8.11/3.74 ms, imaging matrix size = 256 × 256 × 180 mm<sup>3</sup>, slice thickness = 1 mm), fluid-attenuated inversion recovery (FLAIR 2D TR/TE = 11,002/154 ms, MTX = 256 × 256, Slice Thickness = 5 mm; 3D TR/TE = 4800/129 ms, imaging matrix size = 256 × 256 × 180 mm<sup>3</sup>, slice thickness = 1 mm), 2D dual gradient echo (TR/TE1/TE2 = 1000/16/32 ms, MTX 256 × 256 = slice thickness = 3 mm) and quantitative DTI (TR/TE = 9.5 s/66 ms, b-value = 0, 1000 s/mm<sup>2</sup>, number

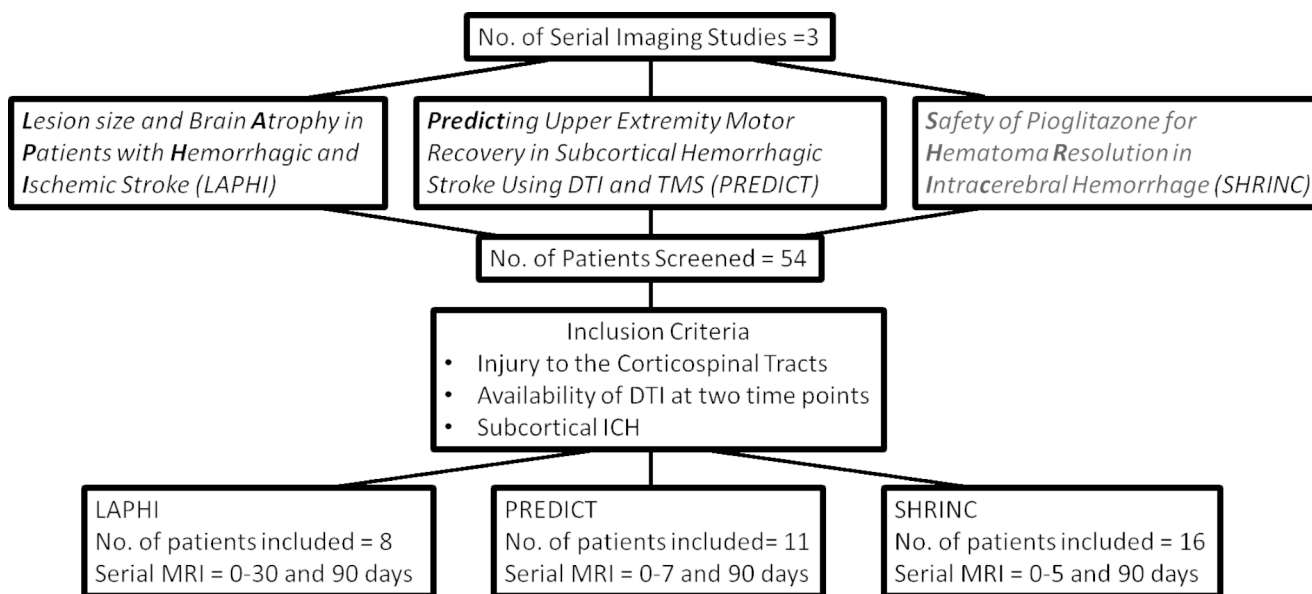


**Fig. 1** Summarize the patient’s cohort in this serial image analysis study

of gradient orientations = 21, image matrix = 128 128, slice thickness = 3 mm). The inpatient DTIs were acquired using 30 directions.

**Image Processing**

The DTI image preprocessing was done using FSL (<http://www.fmrib.ox.ac.uk>), including image alignments, eddy current correction, and skull stripping. The T1-weighted and or FLAIR images were registered to a standard brain image in MNI (Montreal Neurological Institute template) space. The transformation metrics were applied to DTI fractional anisotropy and principal eigenvector V1 maps which were modulated using linear interpolation to create color-coded fractional anisotropy (FA) maps.

**Shape Analysis**

The lesion’s laterality was flipped to aligned ipsilesional and contralesional CST. Using a coronal view of FA color maps, 15 mask/regions of interest (ROI) were drawn across both ipsilesional and contralesional CST, 15 mm apart, originating from pons to cortex at V1 and V2 follow-up MRI as shown in Fig 2 C and Fig 2D. A centroid (i.e., the median of the volume at three intersecting coordinates) of each mask was computed. A control dataset was simulated using the contralesional CST centroid and mirrored to the ipsilesional hemisphere, which was used as the reference shape. For quality assurance, we also compared the centroid displacement using the contralesional CST and a white matter atlas CST template. Overall, using 3-dimensional measurements of the included patients, three sets of data, and 30

coordinates used to define the CST shape in each patient, a total of 9,450 data points were created. The coordinates of the shape were determined via centroid and are referred to as landmarks. The landmark configuration of all patients was subjected to a GPA.

**Generalized Procrustes Analysis (GPA)**

A GPA was used to align all shapes as closely as possible [19]. In the present study, the contralesional CST was used as the reference shape. All other shapes in the sample are superimposed onto the reference shape via translation, rotation, and uniform scaling. A mean shape is computed from the set of superimposed shapes. If the Procrustes distance between the mean shape and the initial reference shape is non-significant, the mean shape makes a new reference, and all patients’ CST shapes are superimposed onto it. The resulting shapes in the sample are precisely superimposed with minimal distance between all landmark coordinate points, and a Principal Component Analysis (PCA) was applied.

**Principal Component Analysis (PCA)**

The Procrustes landmark coordinates were subjected to a PCA to ordinate shapes by arranging in Kendall’s shape space wherein every possible landmark coordinate point was represented by a single point in a multidimensional space [21, 27, 28]. The distances between points in the shape space correspond to the magnitude of the shape differences encompassing all possible variations in the ipsilesional tract (as mapped by the initial landmark coordinate

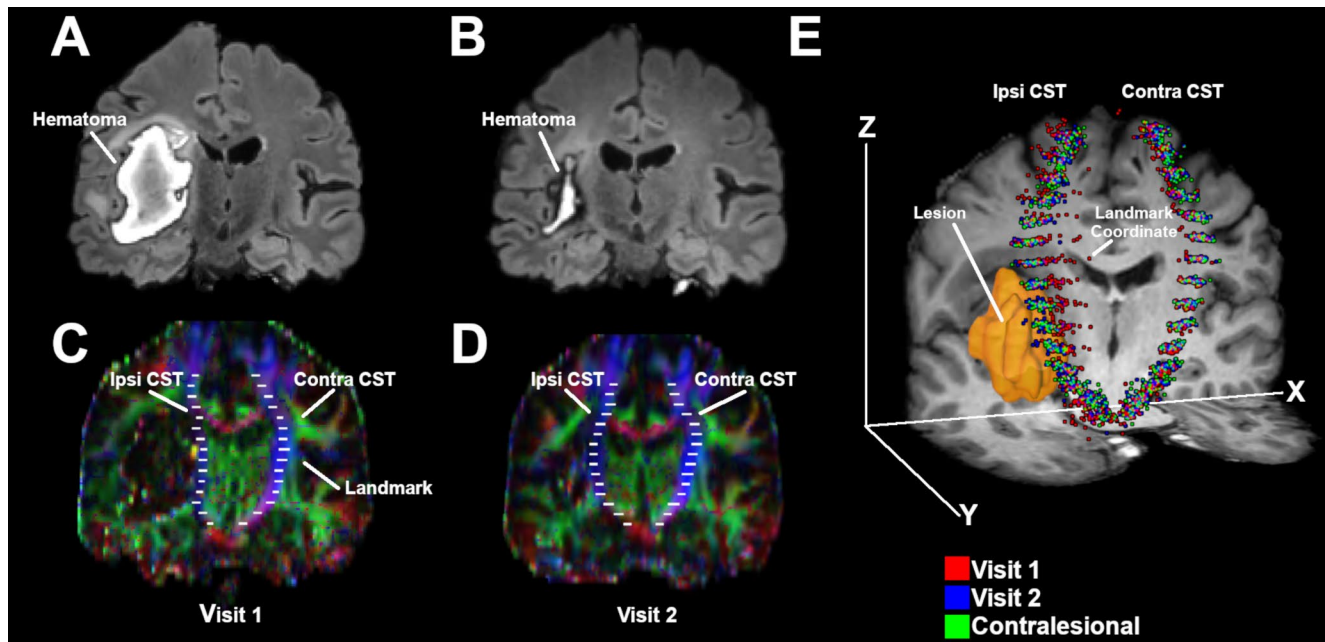


**Fig. 2** Temporal changes in the hematomal tissues and corticospinal tracts (CST) in a representative patient are shown. A significant ( $p < 0.01$ ) reduction in the hematoma volume between visit-1 (A) and visit-2 (B) is shown on a coronal view of a fluid-attenuated inversion recovery. The temporal change in the CST is illustrated by DTI color-coded maps at visit-1 (C) and visit-2 (D). Using principal component

analysis, an overall change in the ipsilesional and contralesional CST shape is depicted in (E) using color code landmarks. At visit-1, the ipsilesional CST (red) shape was significantly ( $p < 0.0001$ ) different in shape than the reference mirrored contralesional (green) shape. At visit -2 (blue), the ipsilesional CST exhibited no significant difference as compared to the reference CST shape

## Statistical Analysis

points). The first three principal components i.e., PC1, PC2, and PC3 captured shape changes along the left-right, anterior-posterior, and superior-inferior orientation respectively. The PC scores were subjected to a multivariate analysis of variance (MANOVA) to evaluate temporal differences in the CST shape variance [22, 29]. Both the GPA and PCA were performed using EVAN-Toolbox software (Version 1.75; EVAN-Society, e.V). In addition, we used generalized linear mixed-effect (GLM) models to associate hematoma volume and NIHSS to the first 10 PC scores over time because these covered a significantly larger percentage of variance.

## Results

### Demographics and Clinical Information

Thirty-five ICH patients, 26 men and 9 women with an average age of  $52.1 \pm 9.4$  years were serially imaged with median MRI time of  $V1=2$  (IQR=1–5) and  $V2=84$  (IQR=56–101) days of onset. All patients had hematoma involving the CST, with 91.1% ( $n=32$ ) originating in the basal ganglia or thalamus whereas the remaining 8.57%

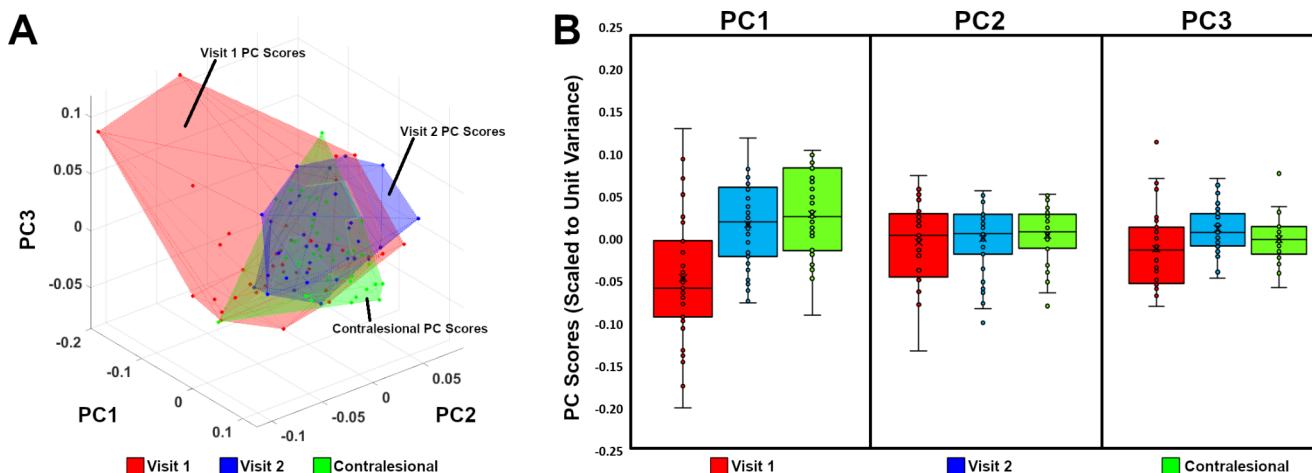
( $n=3$ ) originated in the external capsule, frontoparietal, or frontal lobe. The first MRI (either clinical care or research) revealed parenchyma mass effects in all participants with 85.7% had a midline shift. During the study, 20% of patients exhibited the presence of Wallerian Degeneration identified by asymmetrical MRI signal abnormality in the brain stems. Patients median NIHSS decreased from 13 (IQR=8–16) to 3 (IQR=1–7) between the two imaging time points. The individual patient's demographic and clinical assessment is summarized in Table 1.

Fig-2 A and Fig-2B demonstrate a significant reduction ( $16.37 \pm 27.28$  to  $3.63 \pm 5.01$  cc,  $p < 0.0001$ ) in hematoma volume and temporal change in the ipsilesional CST shape between the two time points after the ICH. Fig-2 C and Fig-2D are DTI color maps showing the deformation and restoration of the ipsilesional CST shape (superior-inferior blue fiber bundle) at baseline and after three months, respectively. The temporal deformation of the ipsilesional CST shape coordinate among all patients is summarized in Fig-2E. Compared to the contralesional CST, the baseline ipsilesional landmarks (red dots) were displaced or deformed as illustrated; however, over time, the CST shape was restored (blue dots) to its pre-ICH location. No significant deformation was noted in the control (green dots) contralesional CST over time.

**Table 1** Patient demographics and clinical assessments

Demographic	Clinical Profile
No of patients enrolled	35
Gender	Male = 26 (74.2%), Female = 9 (25.7%)
Age (years)	52 ± 9.4
Laterality	Left = 17 (53.6%), Right = 18 (51.4%)
Median Baseline NIHSS	15 (IQR = 6–17)
Median NIHSS V1	13 (IQR = 8–16)
Median NIHSS V2	3 (IQR = 1–7)
Median Baseline Blood Pressure (mm of Hg)	198/108 (IQR = (198/108–222/133))
V1 Median MRI (days)	2 (IQR = 1–5)
V2 Median MRI (days)	84 (IQR = 56–99)
Radiological Assessment	
Average Hematoma Volume (cc) at V1 and V2	16.3 ± 27.2 and 3.63 ± 5.05
Location	Basal Ganglia and Thalamus (91.5%) Frontal, Parietal lobe (8.5%)
Median Midline-Shift	85.7%
Mass Effect	100%
Wallerian Degeneration	20%

IQR = Interquartile Range, BP = Blood Pressure, NIHSS = National Institute of Health Stroke Score, V1 = Visit one, V2 = Visit 2



**Fig. 3** Illustrates the temporal changes in ipsilesional CST shape variance in the first three principal components (P1, PC2, and PC3). Using Kendall’s shape space, after principal components analysis, the Procrustes coordinate landmarks are represented as a single point in a multidimensional space. The distance between any given point represents the magnitude of the difference in shape. A illustrates the change in ipsilesional CST shape variance in the PC1, PC2, and PC3 at visit-1 (red) and visit-2 (blue) as compared to the reference shape (green). Fig-A illustrates the change in ipsilesional CST shape variance in the

PC1, PC2, and PC3 at visit-1 (red) and visit-2 (blue), as compared to the reference shape (green). The ipsilesional CST shape variance was 58.3% among the first three principal components’ scores variance. As compared to the reference shape, the baseline shape exhibits significant differences, which were restored at the follow-up imaging. The box plots in B are a quantitative summary of shape variance in the first three PCs with significant ( $p < 0.001$ ) differences in PC1 at the baseline variance shape variance in PC1

**CST Shape Variance**

Fig 3 A illustrates the shape change in individual participants’ ipsilesional CST over time in the first three principal spatial component scores. The reference shape (contralateral CST) is shown in green, where the coordinates were more closely superimposed with minimal distance between the coordinates. At the V1, the ipsilesional CST shape’s coordinates were more dispersed with larger distances, and

minimal superimpose as compared to the reference shape, as shown in Fig 3A (red). At the V2, the ipsilesional shapes were much closer to each other and better superimposed with the reference shape and with no significant difference between them.

The multivariate analysis of variance (MANOVA) showed that the first three principal components account for the majority of variance and are cumulatively responsible for 57.89% of all shape variance. The first principal

component (PC1, left-right) accounts for 36.12% of total ipsilesional CST shape variance, whereas the second (PC2, anterior-posterior) and third (PC3, superior-inferior) are 12.18% and 9.58%, respectively. Significant differences in shape were observed between V1 and V2 at PC1 ( $p < 0.00001$ ) and PC3 ( $p < 0.01$ ) with the greatest variance of  $F = 18.00$  and  $F = 7.271$  respectively. When compared to the contralesional CST at V1, a significant difference in shape was observed only along PC1 ( $p < 0.0000$ ), exhibiting the greatest variance  $F = 24.53$ , and no significant differences were observed at PC2 ( $p = 0.39$ ) and PC3 ( $p = 0.18$ ). However, at V2, all three principal components exhibited

no significant difference as compared to the contralesional CST. These results are summarized in Table 2.

Also, there was no significant difference when comparing the contralesional CST centroid ( $4.47 \pm 1.0$  mm) with the standard brain atlas-based CST template ( $4.25 \pm 1.1$  mm,  $p = 0.62$ ).

Fig-3B illustrates that the PC1 scores of variances were temporally significantly different between the two time points as well as in the contralateral CST shape. The PC3 score of variance was also significantly different between the two time points whereas no significant difference along the PC2 was observed.

**Table 2** Summary of multivariate analysis of variance (MANOVA)

Visit 1 to Visit 2 Comparison					
MANOVA	DF	Pillai	F	DEN DF	Pr (> F)
Time	1	0.28127	8.60960	66	<b>0.0000</b>
Residuals	68				
	DF	Sum Sq	Mean Sq	F	Pr (> F)
PC 1 Time	1	0.07003	0.07003	18.00	<b>0.0000</b>
Residual	68	0.26453	0.00389		
PC 2 Time	1	0.00039	0.00039	0.204	0.6530
Residual	68	0.13050	0.00192		
PC 3 Time	1	0.00991	0.00991	7.271	<b>0.0088</b>
Residual	68	0.09267	0.00136		
Visit 1 to Contralateral Comparison					
MANOVA	DF	Pillai	F	DEN DF	Pr (> F)
Time	1	0.29725	9.30550	66	<b>0.0000</b>
Residuals	68				
	DF	Sum Sq	Mean Sq	F	Pr (> F)
PC 1 Time	1	0.09912	0.09913	24.53	<b>0.0000</b>
Residual	68	0.27483	0.00404		
PC 2 Time	1	0.00107	0.00106	0.722	0.3985
Residual	68	0.10028	0.00147		
PC 3 Time	1	0.00231	0.00231	1.767	0.1882
Residual	68	0.08888	0.00131		
Visit 2 to Contralateral Comparison					
MANOVA	DF	Pillai	F	DEN DF	Pr (> F)
Time	1	0.06355	1.49300	66	0.2246
Residuals	68				
	DF	Sum Sq	Mean Sq	F	Pr (> F)
PC 1 Time	1	0.00252	0.00252	1.004	0.3199
Residual	68	0.17073	0.00251		
PC 2 Time	1	0.00017	0.00016	0.134	0.7157
Residual	68	0.08389	0.00123		
PC 3 Time	1	0.00265	0.00265	3.774	0.0562
Residual	68	0.04775	0.00070		

DF = degrees of freedom; Pillai = Pillai's Trace test statistic; F = F statistic; DEN DF = The number of degrees of freedom associated with the model errors; Pr(> F) = The p-value associated with the F statistic; Sum Sq. = Sum of squares; Mean Sq. = Sum of squares divided by the degrees of freedom.

### CST Shape Variance and Recovery

The GLM indicated that hematoma volume and NIHSS are positively correlated over time whereas PC1 and PC2 exhibited a significant ( $p < 0.05$ ) negative correlation only with hematoma size and not correlated with the NIHSS. These results are summarized in Table 3.

### Discussion

The present study utilized the landmark-based geometrical morphometric method to evaluate the temporal changes in the ipsilesional CST shape and its association with hematoma volume and patient’s neurological deficits after ICH. We used Procrustes analysis to evaluate the change in CST shape after ICH. Unfortunately, high spatial resolution MRI is not routinely integrated as part of a patient’s standard of care, resulting in substantial gaps in our understanding of neuroanatomical damage and potential neurorestoration of specific brain structures. Through serial MRI and the Procrustes analysis, we demonstrated a significant change in the ipsilesional CST shape at the initial time point, which subsequently reverted to its original shape following hematoma and edema resolution. We speculate that the resulting mass effect and increase in ICP, as well as the perihematomal edema growth, were responsible for the CST deformation at the first time point. The restoration of the ipsilesional CST shape indicated that the fibers were either displaced or compressed from their natural location during the acute phase, as shown both quantitatively through DTI color-coded maps and quantitatively via PCA. This phenomenon

is further supported by recent animal studies, where using histology and myelin basic protein immunohistochemistry, the authors showed the presence of white matter fibers within the hematoma cavity up to two months of ICH [30]. Our findings are also consistent with the study by Novakovic et al. among ICH patients in which they demonstrated the presence of white matter within the hematoma that did not decrease at 30-day follow-up [30, 31]. In an exploratory analysis (unpublished data) we also compared the average fractional anisotropy (FA), an imaging metric measure water molecule diffusion hindrance in fibers, in both the ipsilesional and contralesional landmarks. As compared to the contralesional, ipsilesional fiber exhibited significantly lower FA but temporally no significant change between the two time points. Nonetheless, despite the restoration of CST shape, there was no significant correlation with changes in the neurological deficit scale, the NIHSS. This scale was not designed to measure neurological recovery but was the only scale available in our cohort. Furthermore, 20% of patients exhibited anterograde axonal disintegration and demyelination, which hindered recovery. Although Wallerian degeneration (WD) represents a cellular phenomenon, asymmetric MRI signal intensity in the brainstem outside the affected vascular territory and the evidence of cerebral peduncle atrophy are considered hallmarks of WD [32–34]. In future studies, we plan to utilize domain-specific endpoints, such as the Fugl-Meyer score for upper extremity function [35], to further investigate the relationship between ipsilesional CST shape and motor function recovery.

Recent advancements in DTI provided a non-invasive tool to evaluate the microstructural integrity of white matter tracts via a direct or probabilistic tractography method. Using diffusion tensor tractography (DTT) several studies have shown that as compared to the contralesional CST, the ipsilesional CST fibers either failed to propagate or exhibited significantly lower fibers volume [36–40]. However, such studies fail to explain whether lower ipsilesional CST volume is due to fiber loss or inability to propagate because of method limitations. In addition, DTT has been strongly criticized for its subjectivity [41]. Thus, to address this shortcoming, we incorporate a novel non-invasive quantitative morphometric method to predict and evaluate post-stroke recovery. Although in this study we used DTI colormap to place landmarks, however, we do not have to have a DTI colormap for this kind of analysis.

The application of geometric morphometrics, either using thin-plate spline deformation or Procrustes analysis methods, has proven as a viable tool for assessing multiple neurological disorders. For instance, the change in putamen shape has been used as an early biomarker of Parkinson’s disease onset, whereas an altered corpus callosum morphometry has been associated with restless leg

**Table 3** A summary of association among hematoma volume, time, NIHSS, and PC scores

The Fixed Effect of Hematoma Size				
	Estimate	Std. Error	t value	Pr(> z )
(Intercept)	-8.979	0.168	-53.533	0.000
Time V1	10.947	0.184	59.602	<b>0.000</b>
Time V2	9.831	0.163	60.169	<b>0.000</b>
PC 1	-2.814	1.283	-2.194	<b>0.028</b>
PC 2	-5.836	2.556	-2.284	<b>0.022</b>
PC 3	-4.169	2.828	-1.474	0.140
The Fixed Effect of NIHSS				
	Estimate	Std. Error	t value	Pr(> z )
(Intercept)	-9.221	0.117	-78.610	0.000
Time V1	11.744	0.176	66.698	<b>0.000</b>
Time V2	10.648	0.152	69.941	<b>0.000</b>
PC 1	0.828	1.131	0.732	0.464
PC 2	0.268	1.758	0.153	0.879
PC 3	-0.270	2.070	-0.130	0.896

Pr (>|Z|) statistically significant at the significance level of 0.05

syndrome and pyridoxine-dependent epilepsy [25, 42, 43]. Furthermore, a link between the deformation of the temporal lobe and mesial temporal sclerosis as well as the middle cerebral artery geometries and intracranial aneurysms and hippocampus shape and Alzheimer's have been previously documented [24, 44, 45]. Unlike these studies, we evaluated the change in CST shape in all three axis such as left-right, anterior-posterior, and superior-inferior represented by changes in PC1, PC2, and PC3 scores respectively because the hematoma and edema can push or deform CST shape unequally in any axis and therefore we evaluated the change in shape in three-dimension. The significant temporal changes in PC1 scores suggest that predominant CST shape deformation occurred along the right and left rather than anterior-posterior (PC2). The significant change in PC3 scores (superior-inferior) between the two time points substantiates the left-right displacement of CST along PC1. Furthermore, these previous studies employed an atlas-based shape template as a reference shape, which failed to account for age-related atrophy, whereas here we used the contralesional CST as a reference shape to avoid age bias.

Our results also demonstrated a strong association between the change in CST shape variance (PC1 and PC2 score) and hematoma volume. We can speculate that the presence of hematoma affects the shape in both left-right (PC1) and anterior-posterior (PC2) rather than superior-inferior (PC3) directions and such results are in line with non-morphometric studies [46, 47]. In future studies with a larger ICH cohort, we aim to correlate post-stroke brain parenchyma shape deformation to patients' clinical prognosis, ultimately replacing the current rehabilitation concept of one size fits all towards a personalized approach. Furthermore, assessing the type and degree of fiber shape deformation may provide visual guidance to neuro-interventionists for burr holes and needle insertion sites to minimize damage to surrounding healthy tissue. This study has several limitations, including a small sample size and high demographic and pathological variances, such as male-to-female ratio, hematoma sizes, stroke severity, and lack of more fine-grained motor function assessment.

In conclusion, we identified a significant difference in ipsilesional CST shape at the initial time point, which was subsequently restored to its original state. We demonstrated a positive association between the ipsilesional CST shape deformation and hematoma volume, but not recovery maybe 84 days was not an adequate time interval. In future studies, we intend to explore the relationship between CST shape and rehabilitation score as a potential biomarker for post-stroke recovery.

**Acknowledgements** The authors thank Dr. Susan Alderman, Kerry Schneider, and Dorothea Parker for help retrieving clinical and imaging data.

**Author Contributions** SB and MH proposed and developed CST-shaped analysis methods and drafted the manuscript. SS principal investigators of two other ICH studies edited the manuscript. JG, NG, and JA were principal investigators of the pioglitazone clinical trial and edited the manuscript. VM and YL performed the statistical analysis. ES obtained clinical scores and reviewed the manuscript. KH and CS did the radiological assessment, reviewed the data analysis, and edited the manuscript.

## Declarations

**Competing Interests** The authors declare no competing interests. None of the authors has any financial or non-financial interests that are directly or indirectly related to the work submitted for publication.

## References

1. Lahti AM, Nätyнки M, Huhtakangas J, Bode M, Juvela S, Ohtonen P, et al. Long-term survival after primary intracerebral hemorrhage: a population-based case-control study spanning a quarter of a century. *Eur J Neurol*. 2021;28:3663–9.
2. Montaña A, Hanley DF, Hemphill JC. 3rd. Hemorrhagic stroke. *Handb Clin Neurol*. 2021;176:229–48.
3. Leinonen V, Vanninen R, Rauramaa T. Raised intracranial pressure and brain edema. *Handb Clin Neurol*. 2017;145:25–37.
4. Kalita J, Misra UK, Vajpeyee A, Phadke RV, Handique A, Salwani V. Brain herniations in patients with intracerebral hemorrhage. *Acta Neurol Scand*. 2009;119:254–60.
5. Aronowski J, Hall CE. New horizons for primary intracerebral hemorrhage treatment: experience from preclinical studies. *Neurol Res*. 2005;27:268–79.
6. Zhao X, Song S, Sun G, Zhang J, Strong R, Zhang L, et al. Cytoprotective role of haptoglobin in brain after experimental intracerebral hemorrhage. *Acta Neurochir Supplement*. 2011;111:107–12.
7. Yang G, Fan X, Mazhar M, Guo W, Zou Y, Dechsupa N, et al. Neuroinflammation of microglia polarization in intracerebral hemorrhage and its potential targets for intervention. *Front Mol Neurosci*. 2022;15:1013706.
8. Wan J, Ren H, Wang J. Iron toxicity, lipid peroxidation and ferroptosis after intracerebral haemorrhage. *Stroke and vascular neurology*. 2019;4:93–5.
9. An SJ, Kim TJ, Yoon BW. Epidemiology, Risk factors, and clinical features of Intracerebral Hemorrhage: an update. *J stroke*. 2017;19:3–10.
10. Natali AL, Reddy V, Bordoni B, Neuroanatomy. Corticospinal Cord Tract. StatPearls. Treasure Island (FL): StatPearls Publishing Copyright © 2022. StatPearls Publishing LLC.; 2022.
11. Schulz R, Park CH, Boudrias MH, Gerloff C, Hummel FC, Ward NS. Assessing the integrity of corticospinal pathways from primary and secondary cortical motor areas after stroke. *Stroke*. 2012;43:2248–51.
12. Schaechter JD, Perdue KL, Wang R. Structural damage to the corticospinal tract correlates with bilateral sensorimotor cortex reorganization in stroke patients. *NeuroImage*. 2008;39:1370–82.
13. Basser PJ, Mattiello J, LeBihan D. Estimation of the effective self-diffusion tensor from the NMR spin echo. *J Magn Reson Ser B*. 1994;103:247–54.
14. Le Bihan D, Mangin JF, Poupon C, Clark CA, Pappata S, Molko N, et al. Diffusion tensor imaging: concepts and applications. *J Magn Reson Imaging*. 2001;13:534–46.



15. Chaudhary N, Pandey AS, Gemmete JJ, Hua Y, Huang Y, Gu Y, et al. Diffusion tensor imaging in hemorrhagic stroke. *Exp Neurol*. 2015;272:88–96.
16. Yoshioka H, Horikoshi T, Aoki S, Hori M, Ishigame K, Uchida M, et al. Diffusion tensor tractography predicts motor functional outcome in patients with spontaneous intracerebral hemorrhage. *Neurosurgery*. 2008;62:97–103. discussion.
17. Bookstein FL. Landmark methods for forms without landmarks: morphometrics of group differences in outline shape. *Med Image Anal*. 1997;1:225–43.
18. Dryden I, Mardia K, V. (1998) *Statistical Shape Analysis*. New York: Wiley Dryden Statistical shape analysis 1998.
19. Gower JC. Generalized procrustes analysis. *Psychometrika*. 1975;40:33–51.
20. Slice DE. Geometric morphometrics. *Annu Rev Anthropol*. 2007;36:261–81.
21. Zelditch ML, Swiderski DL, Sheets HD. *Geometric morphometrics for biologists: a primer*. 2004.
22. Webster M, Sheets HD. A practical introduction to landmark-based geometric morphometrics. *paleontological Soc papers*. 2010;16:163–88.
23. Urban JE, Maldjian JA, Whitlow CT, Stitzel JD. A method to investigate the size and shape variation of the lateral ventricles with age. *Biomed Sci Instrum*. 2012;48:447–53.
24. Ocakoglu G, Taskapilioglu MO, Ercan I, Demir AB, Hakyemez B, Bekar A, et al. Statistical shape analysis of temporal lobe in mesial temporal sclerosis patients. *Acta Neurochir*. 2015;157:1897–903. discussion 903.
25. Sigirli D, Gunes A, Turan Ozdemir S, Ercan I, Durmus Y, Erdemli Gursel B. Statistical shape analysis of corpus callosum in restless leg syndrome. *Neurol Res*. 2020;42:760–6.
26. Ocakoglu G, Taskapilioglu MO, Altunyuva O, Yilmazlar S. Statistical shape analyses of the Brainstem in Chiari Patients. *Turkish Neurosurg*. 2021;31:618–22.
27. Kendall DG. Shape manifolds, procrustean metrics, and complex projective spaces. *Bull Lond Math Soc*. 1984;16:81–121.
28. Kendall DG, Barden D, Carne TK, Le H. *Shape and shape theory*: John Wiley & Sons; 2009.
29. Willig MR, Owen RD, Colbert RL. Assessment of morphometric variation in natural populations: the inadequacy of the Univariate Approach. *Syst Zool*. 1986;35:195–203.
30. Chen J, Koduri S, Dai S, Toyota Y, Hua Y, Chaudhary N, et al. Intra-hematoma White Matter Tracts Act as a Scaffold for Macrophage Infiltration after Intracerebral Hemorrhage. *Translational stroke research*. 2021;12:858–65.
31. Novakovic N, Linzey JR, Chenevert TL, Gemmete JJ, Troost JP, Xi G et al. White Matter Survival within and around the hematoma: quantification by MRI in patients with Intracerebral Hemorrhage. *Biomolecules*. 2021;11.
32. Domi T, deVeber G, Shroff M, Kouzmitcheva E, MacGregor DL, Kirton A. Corticospinal tract pre-wallerian degeneration: a novel outcome predictor for pediatric stroke on acute MRI. *Stroke*. 2009;40:780–7.
33. Sawlani V, Gupta RK, Singh MK, Kohli A. MRI demonstration of Wallerian degeneration in various intracranial lesions and its clinical implications. *J Neurol Sci*. 1997;146:103–8.
34. Venkatasubramanian C, Kleinman JT, Fischbein NJ, Olivot JM, Gean AD, Eyngorn I, et al. Natural history and prognostic value of corticospinal tract Wallerian degeneration in intracerebral hemorrhage. *J Am Heart Association*. 2013;2:e000090.
35. Fugl-Meyer AR, Jääskö L, Leyman I, Olsson S, Steglind S. The post-stroke hemiplegic patient. 1. A method for evaluation of physical performance. *Scand J Rehabil Med*. 1975;7:13–31.
36. Kumar P, Yadav AK, Misra S, Kumar A, Chakravarty K, Prasad K. Prediction of upper extremity motor recovery after subacute intracerebral hemorrhage through diffusion tensor imaging: a systematic review and meta-analysis. *Neuroradiology*. 2016;58:1043–50.
37. Qiu TM, Zhang Y, Wu JS. Preliminary application of pyramidal tractography in evaluating prognosis of patients with hypertensive intracerebral hemorrhage. *Acta Neurochir Supplement*. 2008;105:165–70.
38. Volbers B, Mennecke A, Kästle N, Huttner HB, Schwab S, Schmidt MA, et al. Quantitative Corticospinal Tract Assessment in Acute Intracerebral Hemorrhage. *Translational stroke research*. 2021;12:540–9.
39. Yoo JS, Choi BY, Chang CH, Jung YJ, Kim SH, Jang SH. Characteristics of injury of the corticospinal tract and corticoreticular pathway in hemiparetic patients with putaminal hemorrhage. *BMC Neurol*. 2014;14:121.
40. McCourt R, Misaghi E, Tu W, Kate M, Gioia L, Treit S, et al. Peri-hematoma corticospinal tract integrity in intracerebral hemorrhage patients: a diffusion-tensor imaging study. *J Neurol Sci*. 2021;421:117317.
41. Chung HW, Chou MC, Chen CY. Principles and limitations of computational algorithms in clinical diffusion tensor MR tractography. *AJNR Am J Neuroradiol*. 2011;32:3–13.
42. Sigirli D, Ozdemir ST, Erer S, Sahin I, Ercan I, Ozpar R, et al. Statistical shape analysis of putamen in early-onset Parkinson's disease. *Clin Neurol Neurosurg*. 2021;209:106936.
43. Oesch G, Maga AM, Friedman SD, Poliachik SL, Budech CB, Wright JN, et al. Geometric morphometrics reveal altered corpus callosum shape in pyridoxine-dependent epilepsy. *Neurology*. 2018;91:e78–e86.
44. Tutino VM, Yan AJ, Veeturi SS, Patel TR, Rajabzadeh-Oghaz H, Waqas M, et al. Landmark-Based shape analysis on Middle Cerebral Intracranial Aneurysms: a geometric Morphometrics Approach to Infer Natural History. *Curr Neurovasc Res*. 2020;17:725–35.
45. Lillemark L, Sørensen L, Pai A, Dam EB, Nielsen M. Brain region's relative proximity as marker for Alzheimer's disease based on structural MRI. *BMC Med Imaging*. 2014;14:21.
46. Farooq S, Shkirkova K, Villablanca P, Sanossian N, Liebeskind DS, Starkman S, et al. National Institutes of Health Stroke Scale correlates well with initial intracerebral hemorrhage volume. *J stroke Cerebrovasc diseases: official J Natl Stroke Association*. 2022;31:106348.
47. Burns JD, Fisher JL, Cervantes-Arslanian AM. Recent advances in the acute management of intracerebral hemorrhage. *Neurosurg Clin*. 2018;29:263–72.

**Publisher's Note** Springer Nature remains neutral with regard to jurisdictional claims in published maps and institutional affiliations.

Springer Nature or its licensor (e.g. a society or other partner) holds exclusive rights to this article under a publishing agreement with the author(s) or other rightsholder(s); author self-archiving of the accepted manuscript version of this article is solely governed by the terms of such publishing agreement and applicable law.